

# Synthesis, Structural and Magnetic Properties of $\text{La}_{0.5}\text{Ba}_{0.5}\text{CoO}_{2.75+x}$

Z. Tan<sup>1,2</sup>, P. Miao<sup>2\*</sup>, Y. Ishikawa<sup>1,2</sup>, M. Hagihala<sup>1,2</sup>, S. Lee<sup>2</sup>,  
S. Torii<sup>2</sup>, M. Yonemura<sup>1,2</sup> and T. Kamiyama<sup>1, 2\*</sup>

<sup>1</sup> Department of Materials Structure Science, Sokendai (The Graduate University for Advanced Studies), Tokai, Ibaraki 319-1106, Japan

<sup>2</sup> Institute of Materials Structure Science, High Energy Accelerator Research Organization (KEK), Tokai, Ibaraki 319-1106, Japan

## ARTICLE INFO

### Article history:

Received 19 December 2017

Received in revised form 26 April 2018

Accepted 26 April 2018

### Keywords:

Cobaltite perovskites

Neutron powder diffraction

Ferromagnetic

Antiferromagnetic

## ABSTRACT

Hole doping to the  $\text{Co}^{3+}$  ion in cobaltite perovskites can significantly modify the electromagnetic properties. The hole-doped cobaltite perovskites  $\text{La}_{0.5}\text{Ba}_{0.5}\text{CoO}_{2.75+x}$  ( $x = 0.08$  and  $x = 0.16$ ) has been prepared by standard solid-state reaction. Neutron powder diffraction and dc-magnetization experiments were performed to investigate the crystal structure and magnetic properties. It is found that both samples have the cubic crystal structure with space group  $Pm\bar{3}m$  in all the measured temperatures. Ferromagnetic transition occurs at 160 K in  $x = 0.16$  sample. For  $x = 0.08$ , found that the short-range ordered ferromagnetic state and a long-range ordered antiferromagnetic state coexist in low temperature.

© 2018 Atom Indonesia. All rights reserved

## INTRODUCTION

The cobaltite perovskites demonstrate many unusual properties such as spin-state transition, metal-insulator transition, large magnetoresistance, negative thermal expansion and so on [1-4]. The Interplay between the spin, charge, orbital, and lattice degrees of freedom has been found to play an essential role. For example, the single perovskite  $\text{LaCoO}_3$  with nominal Co valence being 3+, exhibits the spin-state transition upon heating, where the  $\text{Co}^{3+}$  ion transforms from the low-spin (LS) state ( $t_{2g}^6 e_g^0$ ,  $S = 0$ ) to the high-spin (HS) state ( $t_{2g}^4 e_g^2$ ,  $S = 2$ ) via the intermediate-spin (IS) state ( $t_{2g}^5 e_g^1$ ,  $S = 1$ ) [1,5,6].

There are extensive investigations on the hole-doping effect to  $\text{LaCoO}_3$  through substitution of divalent ion  $A$  ( $A = \text{Ca}, \text{Sr}, \text{Ba}$ ) for La [7]. It is well established that the LS nonmagnetic ground state of  $\text{LaCoO}_3$  undergoes a transition to IS or HS ferromagnetic (FM) state in  $\text{La}_{1-x}\text{A}_x\text{CoO}_3$  [8]. Also, a large magnetoresistance effect has

been reported in  $\text{La}_{1-x}\text{A}_x\text{CoO}_3$  [3]. On the other hand, hole doping to  $\text{Co}^{3+}$  ion can also be introduced by varying the oxygen content, which has not been widely exploited. For example, the nominal valence of Co ion in  $\text{La}_{0.5}\text{A}_{0.5}\text{CoO}_{2.75}$  is 3+, and holes can be filled to the band by increasing the oxygen content. In previous report [9-13], the A-site disordered  $\text{La}_{0.5}\text{Ba}_{0.5}\text{CoO}_{2.75+x}$  ( $x = 0.25$ ), shows FM transition at Curie temperature ( $T_C$ ) 190 K. As the doping decreases to  $x = 0.12$ , the antiferromagnetic (AFM) correlation develops coexists with the FM state at low temperature. When the oxygen content is further lowered to an electron doping side ( $x = -0.15$ ), it shows pure AFM state with the Neel temperature ( $T_N$ ) above room temperature. Since the properties of cobaltite perovskites are very sensitive to chemical compositions (rare-earth element, oxygen content *etc.*) or external stimulus (temperature and pressure *etc.*), this work aims to synthesized the sample  $\text{La}_{0.5}\text{Ba}_{0.5}\text{CoO}_{2.75+x}$  with lighter hole doping level ( $x = 0.08$  and  $x = 0.16$ ) and characterized their magnetic properties by dc magnetization and high-resolution neutron powder diffraction (NPD).

\*Corresponding author.

E-mail address: miao@post.kek.jp; takashi.kamiyama@kek.jp

DOI: <https://doi.org/10.17146/aij.2018.781>

## EXPERIMENTAL METHODS

The samples of  $\text{La}_{0.5}\text{Ba}_{0.5}\text{CoO}_{2.75+x}$  was prepared by standard solid-state reaction. Pre-anneal the  $\text{La}_2\text{O}_3$  oxides at 900 °C to eliminate possible traces of carbon dioxide and water. The raw materials  $\text{La}_2\text{O}_3$ ,  $\text{BaCO}_3$  and  $\text{CoO}$  were mixed with the stoichiometric ratio. The mixed powder was ground and pressed into pellet, followed by heating at 1200 °C in air for 12 h. Temperature increasing and decreasing rate were 2 °C/min. Grinding and heating were repeated for 3 times. We could obtain the single-phase A-site disordered sample  $\text{La}_{0.5}\text{Ba}_{0.5}\text{CoO}_{2.75+x}$  ( $x = 0.16$ ). The sample with  $x = 0.08$  was obtained by annealing the attained samples  $x = 0.16$  under Ar flowing at 250 °C for 12h. We determined the oxygen content by analysis of neutron powder diffraction pattern.

The high-resolution NPD measurement was carried out by Super High Resolution Powder Diffractometer (SuperHRPD) at Materials and Life Science Experimental Facility (MLF), Japan Proton Accelerator Research Complex (J-PARC). The best resolution of SuperHRPD is  $d/d = 0.035\%$  at  $2\theta = 172^\circ$ . The neutron diffraction patterns were analyzed by the Rietveld refinement method using both Z-Rietveld [14,15] and FULLPROF [16]. The magnetization under field cooled (FC) and zero-field cooled (ZFC) was investigated by using a dc superconducting quantum interference device (SQUID) magnetometer (MPMS).

## RESULTS AND DISCUSSION

Figure 1 shows the temperature dependence of magnetization for  $x = 0.08$  and  $x = 0.16$  under 100 Oe. The FC magnetization (see Fig. 1(b)) of  $x = 0.16$  exhibits a ferromagnetic transition at about 160 K. For the sample  $x = 0.08$ , below 130 K the decrease of FC magnetization with decreasing temperature indicates the AFM state at low temperature. However, the divergence between the magnetization of ZFC and FC in Fig. 1(a) and the hysteresis loop of the M/H curve (see the inset) at 13 K suggest that FM state also exists at low temperature. From the view point of phase diagram, at  $x = -0.15$  [10] the sample shows the long range antiferromagnetic order, however as the doping increase to  $x = 0.25$  [9], it exhibits long range FM order. Near the phase boundary of AFM and FM, it is natural to see the coexistence of AFM and FM state, which comes from the electronic origin. Because in vicinity of the boundary, the energy of AFM and FM state is very close.

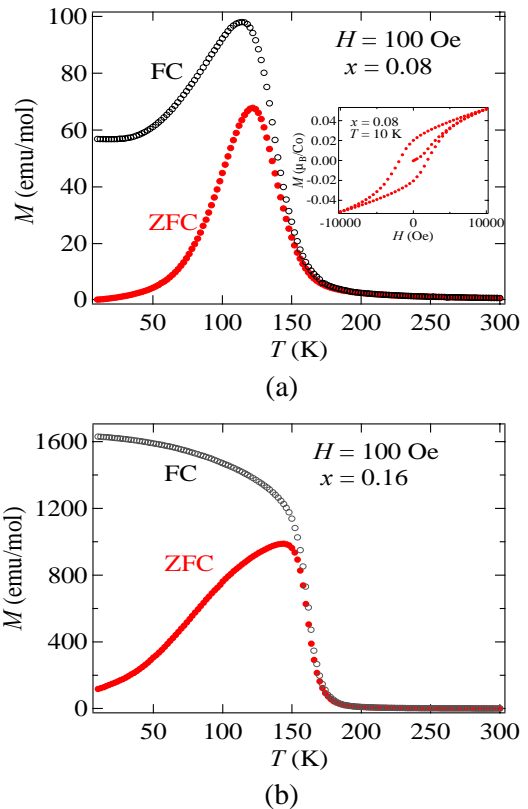


**Fig. 1.** Temperature dependence of magnetization for  $\text{La}_{0.5}\text{Ba}_{0.5}\text{CoO}_{2.75+x}$  under 100 Oe in the ZFC and FC processes respectively (a)  $x = 0.08$ , (b)  $x = 0.16$ . The inset of (a) shows the M/H curve of  $x = 0.08$  sample at 10 K.

The NPD patterns of  $\text{La}_{0.5}\text{Ba}_{0.5}\text{CoO}_{2.75+x}$  ( $x = 0.08$  and  $0.16$ ) were collected by SuperHRPD from 13 K to room temperature. The transition temperature  $T_C = 160$  K for  $x = 0.16$  and  $T_N = 210$  K for  $x = 0.08$  are estimated from the temperature dependence of integrated intensity of the magnetic reflection, as shown in Fig. 2. According to the magnetization data and the integrated intensity, at room temperature both samples are in the paramagnetic state and only nuclear crystal structure contributes to the diffraction pattern. Therefore, the room-temperature pattern of the two samples can be described solely by the nuclear crystal structure, *i.e.*, the cubic structure with the space group  $Pm\bar{3}m$ . No Bragg peak splitting is observed at low temperature, indicating that the crystal structure does not change and remains in the cubic structure with space group  $Pm\bar{3}m$  during the whole temperature range.

From the temperature-dependent NPD pattern of  $x = 0.08$ , we observed the superlattice reflections  $(1/2\ 1/2\ 1/2)$  and  $(3/2\ 1/2\ 1/2)$  initiating at about 210 K upon cooling (see Fig. 2(b)). The superlattice reflections signify the magnetic ordering with propagation vector  $\mathbf{k} = (1/2, 1/2, 1/2)$  and  $T_N = 210$  K. The increase of the magnetic reflection

(1 0 0) intensity in  $\text{La}_{0.5}\text{Ba}_{0.5}\text{CoO}_{2.75+x}$  ( $x = 0.16$ ) upon cooling, indicates the ferromagnetic state with propagation vector  $\mathbf{k} = (0, 0, 0)$  initiates from  $T_C = 160$  K.

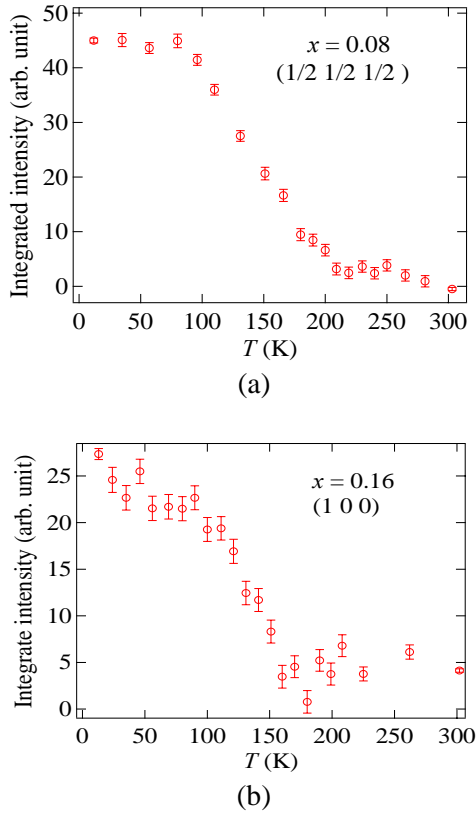


**Fig. 2.** The temperature dependence of integrated intensity of (a) AFM reflection (1/2 1/2 1/2) for  $\text{La}_{0.5}\text{Ba}_{0.5}\text{CoO}_{2.75+x}$  ( $x = 0.08$ ) and (b) the FM reflection (1 0 0) for  $\text{La}_{0.5}\text{Ba}_{0.5}\text{CoO}_{2.75+x}$  ( $x = 0.16$ ).

Using the  $Pm\bar{3}m$  cubic crystal structure and magnetic propagation vector  $\mathbf{k}$ , the symmetry analysis for the magnetic structures has been carried out based on the representation theory. The space group symmetry elements,  $g$ , which leaves the propagation vector  $\mathbf{k}$  invariant was firstly determined. These elements form the little group  $G_{\mathbf{k}}$ . Then the magnetic representation of a crystallographic site can be decomposed in terms of the irreducible representations (IRs) of  $G_{\mathbf{k}}$ :

$$\Gamma_{Mag} = \sum n_{\nu} \Gamma_{\nu}^{\mu}, \quad (1)$$

where  $n$  is the number of times that the IR  $\Gamma_{\nu}$  of order  $\mu$  appears in the magnetic representation  $\Gamma_{Mag}$  for the Co crystallographic site (0.5, 0.5, 0.5). According to Landau theory, the magnetic ordering from a second-order phase transition will condense to a single IR. So the symmetry-allowed magnetic structures corresponds to the non-zero ( $n_{\nu} > 0$ ) IRs of  $G_{\mathbf{k}}$ , from which we can calculate its magnetic basis vectors,  $\mathbf{b}_n$ . The whole calculation was performed using the program *Sarah* [17].

The non-zero IRs and the corresponding basis vectors,  $\mathbf{b}_n$  for the  $x = 0.08$  sample are given in Table 1. Next we carried out the Rietveld refinement using the different combinations of  $\mathbf{b}_n$  so as to determine the magnetic structure. The results for the refinement are listed in Table 2 and fitted pattern is shown in Fig. 3(a), which reveals that the magnetic structure for  $x = 0.08$  sample is the G-type AFM. However, the spin orientation cannot be identified from neutron powder diffraction (Table 2). In the G-type AFM structure, every Co ion aligns antiparallely with the nearest Co neighbors, as shown in the inset of Fig. 3(a). As mentioned above, the magnetization data of the  $x = 0.08$  sample suggests that existence of FM component. Throughout the temperature range, we did not observe any ferromagnetic Bragg peak in the NPD pattern, indicating that there is no long-range ordered FM structure. Therefore, we think the FM state occurs in forms of short range ordering together with a long-range ordered AFM state at low temperature of the  $x = 0.08$  sample.

**Table 1.** The basis vectors of irreducible representations (IRs) for the Co: (0.5, 0.5, 0.5) of the  $x = 0.08$  sample. The crystal structure is cubic  $Pm\bar{3}m$  and the magnetic propagation vector  $\mathbf{k}$  is (1/2, 1/2, 1/2).

IRs	Basis Vectors	
	$\Gamma_7$	1
	2	(1 0 0)
	3	(0 1 0)

**Table 2.** Refined magnetic moments ( $\mu_B$ ) for the Co ion of the  $x = 0.08$  sample based on the basis vectors from Table 1.  $R_M$  is the magnetic  $R$  factor for Rietveld refinement.

Model	1	1+ 2	1+ 2+ 3
$m_x$	0	1.05	0.86
$m_y$	0	0	0.86
$m_z$	1.49	1.05	0.86
$m_{tot}$	1.49	1.49	1.49
$R_M$ (%)	6.71	6.65	6.66

For  $x = 0.16$ , we also perform the symmetry analysis with propagation vector  $\mathbf{k} = (0, 0, 0)$ . The resultant non-zero IRs and the corresponding basis vectors,  $\mathbf{b}_n$  are presented in Table 3. The result of Rietveld refinement using the different combinations of  $\mathbf{b}_n$  are listed in Table 4. Finally, the simple FM structure was found for  $x = 0.16$  as depicted in the inset of Fig. 3(b) and the fitted pattern is shown in Fig. 3(b). Also, we cannot determine the spin orientation by neutron powder diffraction (Table 4). In the NPD pattern of  $\text{La}_{0.5}\text{Ba}_{0.5}\text{CoO}_{2.75+x}$  ( $x = 0.16$ ) at low temperature we could not observe reflections (1/2 1/2 1/2) and (3/2 1/2 1/2). So, there is no long-range ordered AFM state at low temperature in this sample. It has been reported that FM state and small AFM clusters coexist in ground state in  $\text{La}_{0.5}\text{Ba}_{0.5}\text{CoO}_{2.75+x}$

( $x = 0.25$ ) [18]. In case of  $x = 0.16$ , a short-range ordered AFM state, which cannot be detected by NPD, may coexist with the long-range ordered FM state at low temperature as well. To clarify whether there is short-range ordered AFM state at low temperature, further experiments are needed, such as the muon-spin-relaxation experiment.

**Table 3.** The basis vectors of irreducible representations (IRs) for the Co: (0.5, 0.5, 0.5) of the  $x = 0.16$  sample. The crystal structure is cubic  $Pm\bar{3}m$  and the magnetic propagation vector  $k$  is (0, 0, 0).

IRs	Basis Vectors	
	1	(0 0 1)
$\Gamma_{10}$	2	(1 0 0)
	3	(0 1 0)

**Table 4.** Refined magnetic moments ( $\mu_B$ ) for the Co ion of the  $x = 0.16$  sample based on the basis vectors from Table 3.  $R_M$  is the magnetic  $R$  factor for Rietveld refinement.

Model	1	1 <sup>+</sup>	2	1 <sup>+</sup>	2 <sup>+</sup>	3
$m_x$	0	1.25			1.02	
$m_y$	0	0			1.02	
$m_z$	1.77	1.25			1.02	
$m_{tot}$	1.77	1.77			1.77	
$R_M$ (%)	8.40	8.63			8.41	

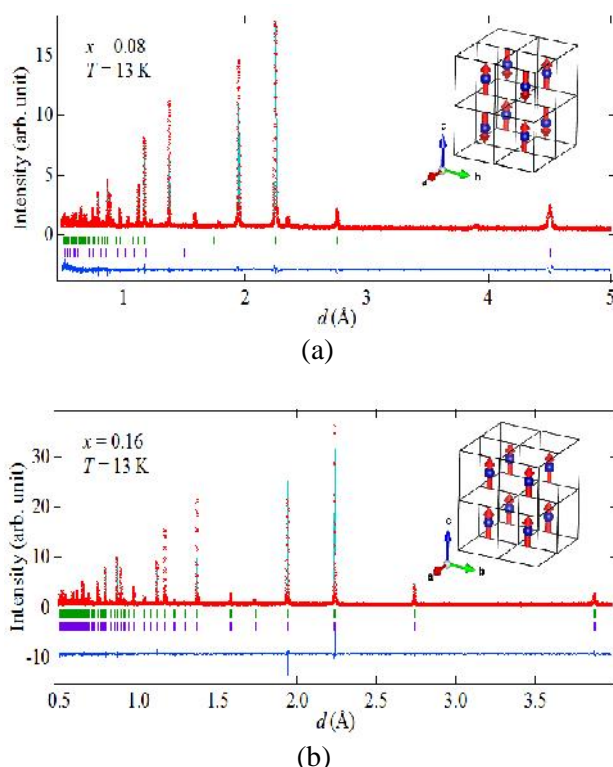


**Fig. 3.** The NPD patterns of  $\text{La}_{0.5}\text{Ba}_{0.5}\text{CoO}_{2.75+x}$  (a)  $x = 0.08$ , (b)  $x = 0.16$  were collected at 13 K. The observed and calculated patterns are shown at the top with the cross markers and the solid line, respectively. The vertical green and purple marks in the middle show positions calculated of Bragg reflections for nuclear and magnet diffraction, respectively. The bottom blue line represents the difference between observed and calculated intensities. The inset of (a) and (b) shows the G-types AFM and FM structure, respectively. For clarity only Co is displayed.

## CONCLUSION

The A-site disordered perovskite cobaltite,  $\text{La}_{0.5}\text{Ba}_{0.5}\text{CoO}_{2.75+x}$  ( $x = 0.08, 0.16$ ) has been successfully synthesized by solid state reaction. The refinement result of the NPD shows that the crystal structures remain in the cubic structure with space group  $Pm\bar{3}m$  in the temperature range of 13 K to room temperature. The  $x = 0.16$  sample shows FM state at low temperature with the transition at 160 K. For the  $x = 0.08$  sample, the short-range ordering FM state occurs together with a long-range ordered AFM state at low temperature. The sample with  $x = 0.08$  shows a similar magnetic behavior with the sample  $x = 0.05$ . By increasing the doping slightly from  $x = 0.12$  to  $x = 0.16$ , it leads to the change from two phases with coexistence of long range order AFM and FM to only one phase with long range order FM.

## ACKNOWLEDGMENT

The neutron diffraction experiments were carried out in S-type research project, KEK (2014S05) at MLF, J-PARC. We would like to appreciate Kaoru Namba, Masahiro Shioya, Taketo Moyoshi and Katsumi Shimizu for their technical assistance.

## REFERENCES

1. M.A. Señarís-Rodríguez and J.B. Goodenough, *J. Solid State Chem.* **116** (1995) 224.
2. Y. Moritomo, M. Takeo, X.J. Liu, T. Akimoto and A. Nakamura, *Phys. Rev. B* **58** (1998) R13334.
3. G. Briceño, H. Chang, X. Sun *et al.*, *Science* **270** (1995) 273.
4. P. Miao, X. Lin, A. Koda *et al.*, *Adv. Mater.* **29** (2017) 1605991.
5. T. Saitoh, T. Mizokawa, A. Fujimori *et al.*, *Phys. Rev. B* **55** (1997) 4257.
6. K. Asai, A. Yoneda, O. Yokokura *et al.*, *J. Phys. Soc. Jpn.* **67** (1998) 290.
7. M. Kriener, M. Braden, H. Kierspe *et al.*, *Phys. Rev. B* **79** (2009) 224104.
8. M.A. Señarís-Rodríguez and J.B. Goodenough, *J. Solid State Chem.* **118** (1995) 323.
9. T. Nakajima, M. Ichihara and Y. Ueda, *J. Phys. Soc. Jpn.* **74** (2005) 1572.

10. V. Sikolenko, V. Efimov, I.O. Troyanchuk *et al.*, J. Phys. Conf. Ser. **391** (2012) 012106.
11. I.O. Troyanchuk, M.V. Bushinsky, V. Sikolenko *et al.*, Eur. Phys. J. B **86** (2013) 435.
12. I.O. Troyanchuk, D.V. Karpinsky, M.V. Bushinsky *et al.*, J. Appl. Phys. **112** (2012) 013916.
13. I.O. Troyanchuk, D.V. Karpinsky, M.V. Bushinsky *et al.*, JETP Lett. **93** (2011) 139.
14. R. Oishi, M. Yonemura, Y. Nishimaki *et al.*, Nucl. Instrum. Methods Phys. Res., Sect. A **600** (2009) 94.
15. R. Oishi-Tomiyasu, M. Yonemura, T. Morishima *et al.*, J. Appl. Crystallogr. **45** (2012) 299.
16. J. Rodríguez-Carvajal, Physica B (Amsterdam, Neth.) **192** (1993) 55.
17. A. Wills, Physica B (Amsterdam, Neth.) **278** (2000) 680.
18. Devendra Kumar and A Banerjee, J. Phys.: Condens. Matter **25** (2013) 216005.